

Pressure and magnetic-field effects on a quasi-2D spin- $1/2$ Heisenberg antiferromagnet

N. Barbero,¹ T. Shiroka,^{1,2,*} C. P. Landee,³ M. Pikulski,¹ H.-R. Ott,^{1,2} and J. Mesot^{1,2}

¹Laboratorium für Festkörperphysik, ETH Zürich, CH-8093 Zurich, Switzerland

²Paul Scherrer Institut, CH-5232 Villigen PSI, Switzerland

³Department of Physics, Clark University, Worcester, Massachusetts 01610, USA

$\text{Cu}(\text{pz})_2(\text{ClO}_4)_2$ (with *pz* denoting pyrazine, $\text{C}_4\text{H}_4\text{N}_2$) is among the best realizations of a two-dimensional spin- $1/2$ square-lattice antiferromagnet. Below $T_N = 4.21$ K, its weak interlayer couplings induce a 3D magnetic order, strongly influenced by external magnetic fields and/or hydrostatic pressure. Previous work, focusing on the $[H, T]$ phase diagram, identified a spin-flop transition, resulting in a field-tunable bicritical point. However, the influence of external pressure has not been investigated yet. Here we explore the extended $[p, H, T]$ phase diagram of $\text{Cu}(\text{pz})_2(\text{ClO}_4)_2$ under pressures up to 12 kbar and magnetic fields up to 7.1 T, via magnetometry and ^{35}Cl nuclear magnetic resonance (NMR) measurements. The application of magnetic fields enhances T_{XY} , the crossover temperature from the Heisenberg to the XY model, thus pointing to an enhancement of the effective anisotropy. The applied pressure has an opposite effect [$dT_N/dp = -0.050(8)$ K/kbar], as it modifies marginally the interlayer couplings, but likely changes more significantly the orbital reorientation and the square-lattice deformation. This results in a remodeling of the effective Hamiltonian, whereby the field and pressure effects compensate each other. Finally, by comparing the experimental data with numerical simulations we estimate T_{BKT} , the temperature of the Berezinskii-Kosterlitz-Thouless topological transition and argue why it is inaccessible in our case.

PACS numbers: 75.40.Cx, 75.10.Jm, 62.50.-p, 67.80.dk

I. INTRODUCTION

The antiferromagnetic coupling of magnetic moments in materials with low-dimensional sub-units gives rise to interesting phenomena, including the Haldane gap, the quantum spin-liquid state, topological phase transitions, etc.¹ Such systems comprise both one- (chains and ladders), as well as two-dimensional (triangular-, square-, and rectangular) spin arrangements, which can be realized by synthesizing the relevant materials. These can serve as playgrounds for testing key theoretical concepts, such as those of quantum phase transitions and criticality.² In addition, studies of quantum magnets and spin-wave dynamics promise new applications in the fields of magnonics and spintronics,³ where the use of antiferromagnets (AFMs) may serve to improve magnetic-storage capabilities.⁴

The two-dimensional Heisenberg-type cuprates deserve special attention, since their weakly-interacting layers, characterized by a square-lattice disposition of Cu(II) ions, display remarkable structural and magnetic analogies with the copper-oxide high- T_c superconductors, such as, e.g., $\text{La}_{2-x}\text{Sr}_x\text{CuO}_4$. In this work we focus on $\text{Cu}(\text{pz})_2(\text{ClO}_4)_2$, a prototype material with properties that are governed by the competition between order and quantum fluctuations, normally encountered in materials featuring well-isolated layers.⁵ Indeed, as a 2D quasi-Heisenberg antiferromagnet (QHAF), $\text{Cu}(\text{pz})_2(\text{ClO}_4)_2$ exhibits quantum phase transitions, accessible by varying external parameters,⁶ such as applied magnetic fields or the hydrostatic pressure.

Several experimental techniques have been used to investigate the magnetic properties of $\text{Cu}(\text{pz})_2(\text{ClO}_4)_2$ in magnetic fields ranging from 0 to 13.5 T, including zero-field muon-spin resonance (μSR),⁷ specific-heat,^{7,8} neutron scattering,⁸ ESR,⁹ and magnetization⁹ measurements. The essential structural entities of $\text{Cu}(\text{pz})_2(\text{ClO}_4)_2$ consist of layers of Cu(II) ions with spin $S = 1/2$, arranged on a square lattice (see Fig. 1). The neighboring layers are bridged by four pyrazine ligands and their stacking involves a $(1/2, 1/2)$ unit-cell shift along the square diagonal.¹⁰ The perchlorate counterions are semicoordinate in the axial sites, such that the Cu(II)-ions adopt a nearly tetragonal arrangement,

with a clear separation between the layers.⁵ In $\text{Cu}(\text{pz})_2(\text{ClO}_4)_2$ the intra-layer interactions are dominated by the nearest-neighbor (NN) interaction among Cu(II) ions, initially estimated as $J/k_B = 18.1$ K from dispersion curves of inelastic neutron scattering.⁸ Subsequently, Density Functional Theory (DFT) simulations showed that a tiny difference in the Cu–Cu bond lengths ($d_1 = 6.898$ Å vs. $d_2 = 6.876$ Å) is reflected in two distinct NN exchange couplings, with $J_1/J_2 = 1.4$.¹¹ By taking into account these different NN interaction strengths, the magnetic-interaction pattern of $\text{Cu}(\text{pz})_2(\text{ClO}_4)_2$ can be visualized as a succession of zigzag interaction paths (see Fig. 1). In addition, the same simulations predict a rather weak next-nearest neighbor (NNN) interaction, $J_3/k_B = 0.4$ K, implying a weak degree of frustration in the system. Concerning the interlayer couplings, the excellent layer separation is confirmed by the low value of the J_{int} interaction ($J_{\text{int}}/J = 8.8 \cdot 10^{-4}$).⁸ Nevertheless, this residual interaction is strong enough to induce a transition from a 2D quasi-Heisenberg AFM to a 3D ordered Néel state at a relatively high value of $T_N = 4.21$ K.¹²

In this work we primarily aimed at exploring the $[p, T]$ phase diagram of $\text{Cu}(\text{pz})_2(\text{ClO}_4)_2$, an investigation complementary to the $[H, T]$ mapping of the same compound reported recently.⁹ The presence of organic units in $\text{Cu}(\text{pz})_2(\text{ClO}_4)_2$, generally easily deformable under pressure, makes it a suitable candidate for studying the role of pressure and its influence on the strength of the different exchange interactions in an almost ideal 2D quantum-spin system. In addition, we aimed also at investigating the combined influence of external pressure and magnetic fields, as well as at exploring the possibility of observing the renowned Berezinskii-Kosterlitz-Thouless (BKT) topological transition^{13,14} in the low- T XY phase. In the following, we present the results of magnetometry (Sec. III A) and magnetic-resonance experiments (Sec. III B), and discuss how the magnetic anisotropy, inter-, and intra-layer couplings are modified under the joint application of pressure and magnetic field. The unexpected compensation effects we observe, seem to arise from the contrasting roles played by the deformation of the 2D square lattice and the

reorientation of the electronic orbitals of in-plane ions.

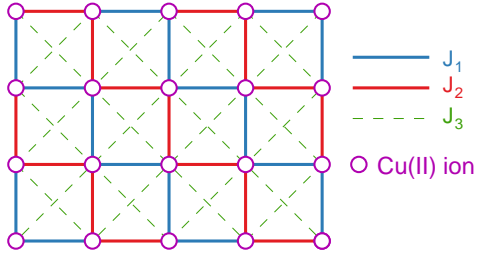


FIG. 1. (Color online) A layer of the 3D $\text{Cu}(\text{pz})_2(\text{ClO}_4)_2$ structure, showing the Cu(II) ions (circles) arranged on a square lattice. The nearest-neighbor exchange interactions, forming a stripy succession of J_1 and J_2 (full lines), are the dominant ones. The diagonal NNN J_3 interactions (dashed lines) are weaker.

II. EXPERIMENTAL DETAILS

Single crystals of $\text{Cu}(\text{pz})_2(\text{ClO}_4)_2$ were synthesized by dissolving $\text{Cu}(\text{ClO}_4)_2 \cdot 6\text{H}_2\text{O}$ and pyrazine in water to which a drop of dilute $\text{HClO}_4(\text{aq})$ was added [the latter prevents the precipitation of $\text{Cu}(\text{OH})_2$ and CuCO_3].¹⁵ The solution was then left to evaporate, with the crystals growing on a timescale of weeks. Eventually the mixture was filtered and the recovered crystals washed in cold deionized water and left to dry in air. Since the samples are air- and water sensitive, they were constantly kept in a desiccator.¹⁵ Three samples with different sizes were available: one large sample (81 mg, $6.5 \times 5 \times 1 \text{ mm}^3$) was used for the zero-pressure magnetometry, whereas the smaller ones (14 and 5.5 mg) were employed for the NMR and magnetization measurements under pressure. The single $\text{Cu}(\text{pz})_2(\text{ClO}_4)_2$ crystals were cut such as to have two opposite faces parallel to the bc planes. This allowed us to align the samples with their a axis (*hard* magnetic axis) parallel to the applied magnetic field with an uncertainty of a few degrees.

The SQUID magnetometry measurements at zero pressure were carried out using a commercial Magnetic Property Measurement System (MPMS) setup from Quantum Design, equipped with a 5.5 T-magnet. For the NMR investigations of $\text{Cu}(\text{pz})_2(\text{ClO}_4)_2$, i.e., line- and spin-lattice relaxation measurements at 7.063 T, the ^{35}Cl nucleus proved to be the most suitable for our study. Typically, we employed standard spin-echo sequences, consisting in $\pi/2$ and π pulses of 2 and $4 \mu\text{s}$, respectively, with a recycle delay ranging from 0.2 to 0.6 s, depending on temperature. The narrow lines at low pressure were obtained by the FFT of the echo signal, while the broader high-pressure lines were acquired by sweeping the frequency and summing the resulting FFT data. A limited number of scans (from 256 to 1024) was sufficient for acquiring signals with a good S/N ratio. The ^{35}Cl NMR signal of an aqueous NaCl solution at 29.467 MHz (measured separately at room temperature) served as a frequency reference.

For the hydrostatic pressure studies, two high-pressure cells were built, with bodies and nuts consisting of high-purity, low-magnetic-response BeCu and bores of 5 and 2.7 mm for the NMR and SQUID-magnetometry measurements, respectively. The feedthrough assembly of the NMR pressure cell was constructed using a hardened MP35N alloy, while the piston consisted of tungsten carbide (WC).¹⁶ The leads were insulated copper wires with a diameter of

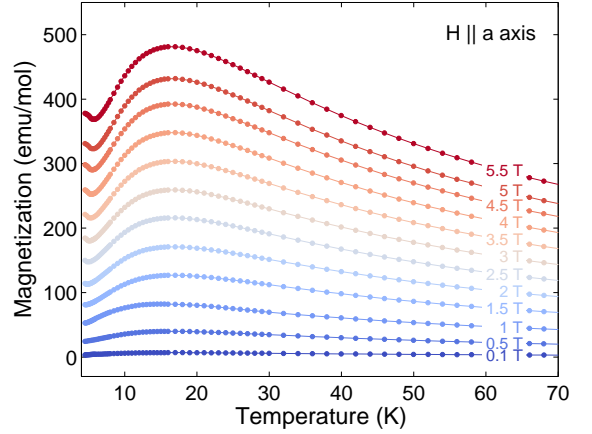


FIG. 2. (Color online) Magnetization $M(T)$ curves collected at different magnetic fields (from 0.1 to 5.5 T), applied along the a axis.

0.1 mm. Once inserted in the NMR coil, the specimen was embedded into a PTFE container filled with silicon oil. In addition, a secondary coil, containing a powdered, high-purity Cu(I)-oxide sample mixed with paraffin wax and serving as an in-situ pressure gauge, was also inserted into the container, which was then sealed with the feedthrough unit. The pressurization was performed by means of an industrial press (25-T Enerpac), with which pressures up to 18 kbar were achieved at room temperature (decreasing by ca. 25% at low temperatures). The pressure gauge was calibrated via ^{63}Cu NQR measurements, following established references.¹⁷ The ^{63}Cu NQR signal in Cu_2O was acquired using a spin-echo sequence with a recycle delay of 60 s. The pressure cell used in the SQUID magnetometer had a similar piston-design as the NMR cell. However, due to magnetometer-related dimensional constraints, only pressures up to about 12 kbar could be reached in this case. In the high-pressure region of the cell, the sample and the pressure gauge, in the form of a 1-mg piece of lead, were separated by a quartz-rod spacer. The in-situ pressure was monitored by measuring the superconducting transition of lead, by considering its known T_c -vs.-pressure dependence.¹⁸

III. EXPERIMENTAL RESULTS AND DISCUSSION

A. SQUID magnetometry

1. Magnetic field effects on magnetization

In Fig. 2 we display the results of measurements of the temperature dependence of the magnetization $M(T)$ of $\text{Cu}(\text{pz})_2(\text{ClO}_4)_2$ between 4.5 K and room temperature at different external magnetic fields, from 0.1 T up to 5.5 T. From these data we extracted three distinct temperatures: T_{max} , T_{min} , and T_{N} , as indicated in Fig. 3.

The values of T_{max} , determined from parabolic fits to the data around the magnetization maximum, can be related with the results of high-temperature series expansion calculations,¹⁹ or to those of more recent numerical simulations,²⁰ which for a 2D Heisenberg spin- S system predict $k_{\text{B}}T_{\text{max}}/J = 1.12S(S+1) + 0.10$ and $k_{\text{B}}T_{\text{max}}/J = 0.936$, respectively. By considering the average experi-

mental value $T_{\max} \approx 17\text{K}$, we obtain an average value for the in-plane exchange-interaction parameter $J/k_B = 18.2\text{K}$, in excellent agreement with the above-mentioned $J/k_B = 18.1\text{K}$, derived from neutron-scattering data.⁸ This suggests that, at temperatures above 10 K, the system may be modeled as an isotropic two-dimensional Heisenberg antiferromagnet (HAFM). In order to check this assumption we performed Quantum Monte Carlo (QMC) simulations on a $L \times L$ lattice, with $L = 256$ sites, based on the ALPS package²¹ and using the above mentioned J as the only parameter. As shown in Fig. 3, for $T > 10\text{K}$ the calculated $\chi(T)$ dependence is in very good agreement with experimental susceptibility data, thus confirming the above-mentioned 2D-model assumption, while the simulation clearly fails to reproduce the data at lower temperatures. In two-dimensional spin- $1/2$ HAFMs, a minimum in $\chi(T)$ is claimed to indicate in-plane exchange anisotropies Δ_{XY} which, even when tiny, may induce a crossover from a Heisenberg to an XY regime.²²

As we shall see below, the 3D ordering temperature T_N may accurately be determined by measurements of the NMR spin-lattice relaxation rate $T_1^{-1}(T)$. The evaluation of T_N from the $\chi(T)$ data, however, is not straightforward. In a previous work,²³ it was claimed that the inversion point in $\chi(T)$ below T_{\min} provides a reliable estimate of T_N . For our purposes, mainly to monitor the variation of T_N upon changing the magnitude of the external magnetic field, we have chosen the approach indicated in the inset of Fig. 3. Here we estimate T_N by a parabolic fit to the data at the lower end of the covered temperature range and its extrapolation to the minimum value in $\chi(T)$.

Following the approach outlined in earlier work on $\text{Sr}_2\text{CuO}_2\text{Cl}_2$,²⁴ another model compound for 2D magnetic systems, we distinguish three regions in the low-temperature range of $\chi(T)$, i.e., $T < T_N$, $T_N < T < T_{\min}$, and $T > T_{\min}$. Above approximately 10 K, i.e., distinctly above T_{\min} , $\text{Cu}(\text{pz})_2(\text{ClO}_4)_2$ may be regarded as a 2D $S = 1/2$ HAFM. In a narrow temperature range just below T_{\min} , the system adopts an intermediate disordered XY phase, which undergoes a 3D ordering at T_N . It was empirically established that the crossover temperature T_{XY} , that we tentatively set equal with T_{\min} , may be estimated by:²⁴

$$T_{XY} = \frac{4\pi \cdot 0.214 \cdot J}{\ln(160/\Delta_{XY})}, \quad (1)$$

where Δ_{XY} is the intrinsic in-plane exchange anisotropy. Eq. 1 implies that T_{XY} varies linearly with J , but tends to saturate at small Δ_{XY} values. By inserting the values of $T_{XY} \approx T_{\min}$ we obtain values for Δ_{XY} of the order of 10^{-3} to 10^{-2} . More specifically, we note that an increase of the magnetic field enhances the resulting value of Δ_{XY} , which rises from 6×10^{-3} at 2 T to 2.4×10^{-2} at 4 T. Given the tiny in-plane exchange anisotropy Δ_{XY} of $\text{Cu}(\text{pz})_2(\text{ClO}_4)_2$ (see above), it is of interest to investigate its low-temperature behavior in detail.

In order to capture the influence of external magnetic fields on the low-temperature magnetic features of $\text{Cu}(\text{pz})_2(\text{ClO}_4)_2$, one can use a general Hamiltonian \mathcal{H} , which includes an applied magnetic field H , NN and NNN interactions (J_{NN} and J_{NNN} , respectively), and a generic exchange

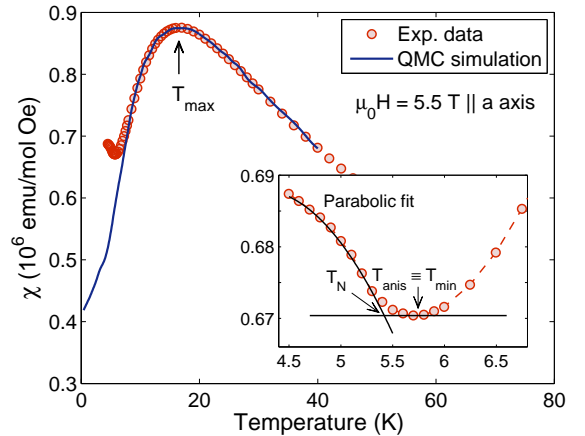


FIG. 3. (Color online) Comparison of the temperature-dependent magnetic susceptibility (dots) with Quantum Monte Carlo (QMC) simulations of a uniform susceptibility model (line). The simulations were carried out on an $L \times L$ lattice, with $L = 256$ sites, based on the ALPS package using the Stochastic Series Expansion (SSE) method. Inset: Close-up view of the magnetic susceptibility curve, showing the definitions of T_N and T_{\min} .

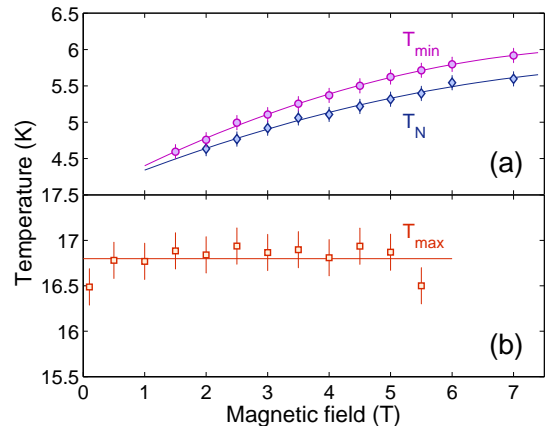


FIG. 4. (Color online) Metadata from Fig. 2 showing (a) the evolution of T_{\min} , T_N , and of (b) T_{\max} with the applied magnetic field at $p = 0$ kbar. While T_{\min} and T_N gradually increase with the field, T_{\max} remains practically constant.

anisotropy parameter Δ_{XY} .⁸

$$\begin{aligned} \mathcal{H} = & J_{\text{NN}} \sum_{\langle i,j \rangle} [S_i^x S_j^x + S_i^y S_j^y + (1 - \Delta_{XY}) S_i^z S_j^z] \\ & + J_{\text{NNN}} \sum_{\langle i,k \rangle} \mathbf{S}_i \cdot \mathbf{S}_k - g\mu_B H \sum_i S_i^z. \end{aligned} \quad (2)$$

For $\Delta_{XY} = 0$ Eq. (2) reproduces the Heisenberg case, while for $\Delta_{XY} = 1$ it depicts the XY model. Earlier numerical simulation studies of the two-dimensional XY model predicted a significant upturn in the magnetic susceptibility when T_{BKT} is approached.²⁵ This behavior was observed experimentally in $\text{Sr}_2\text{CuO}_2\text{Cl}_2$,²⁴ where the susceptibility data and numerical simulations were found to be in good agreement. A short discussion on the observability of a BKT transition in our case is given in Sec. IV. From the data shown in Fig. 2 it may be inferred that the crossover from the Heisenberg to XY behavior and the transition to a 3D magnetic order both shift to higher temperatures with increasing magnetic field (see Fig. 4). The main cause for the first is most

likely a growing anisotropy with increasing field, while for the second a field-induced reduction of quantum fluctuations. This conclusion reflects the fact that higher magnetic fields enhance the trend for order, quench the quantum fluctuations, and enhance the anisotropy, such that the field orientation imposes the energetically-favorable direction. As expected, the value of J , related to T_{\max} , is essentially field independent.

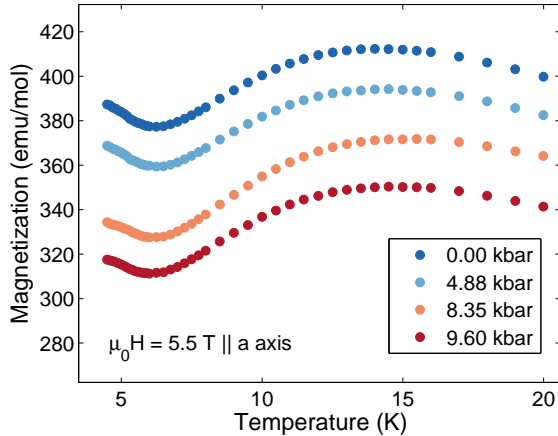


FIG. 5. (Color online) Magnetization M vs. temperature for different applied pressures (from 0 to 9.60 kbar). Data were acquired in an external magnetic field of 5.5 T, parallel to the a axis and subsequently corrected for a small contribution to $M(T)$ of the empty pressure-cell body.

2. Influence of external pressure

As an example of the influence of external hydrostatic pressure at a fixed magnetic field, we show a corresponding $M(T)$ data set at selected pressures in a field of 5.5 T in Fig. 5. On the basis of such data, we evaluated the pressure dependence of T_N , T_{\min} , and T_{\max} for a selection of external fields; the overall results are displayed in Fig. 6.

As we mentioned above, an exact determination of T_N from $M(T)$ data is not straightforward. Nevertheless, an acceptable way to estimate T_N is indicated in the inset of Fig. 3. Following this procedure, we obtain a clear trend of $T_N(p)$, which, in a field of 5.5 T, decreases monotonously from 5.4 K at $p = 0$ to 4.8 K at $p = 9.6$ kbar [see Fig. 6(a)].

Similarly, from panel (b) of this figure it may be seen that at low fields also $T_{\min} \approx T_{XY}$ decreases with increasing pressure. At higher fields, the pressure-induced shifts of T_{\min} are clearly reduced in magnitude with no distinct trend. Quite generally, the effect of external pressure on the $M(T)$ curve of $\text{Cu}(\text{pz})_2(\text{ClO}_4)_2$ is rather weak. Nevertheless, the trends in $T_{\min}(p)$ and $T_{\max}(p)$ observed in low external fields seem to be weakened in elevated fields.

In a first approach, to interpret the observed pressure effects on T_N , one can use the Ehrenfest relation for second-order phase transitions:²⁶

$$\frac{dT_N}{dp} = \frac{TV_m \Delta\beta}{\Delta C_p}. \quad (3)$$

Here p is the pressure, V_m the molar volume, C_p the specific heat at constant pressure, and β the volumetric coefficient of thermal expansion. The quantities $\Delta\beta$ and ΔC_p

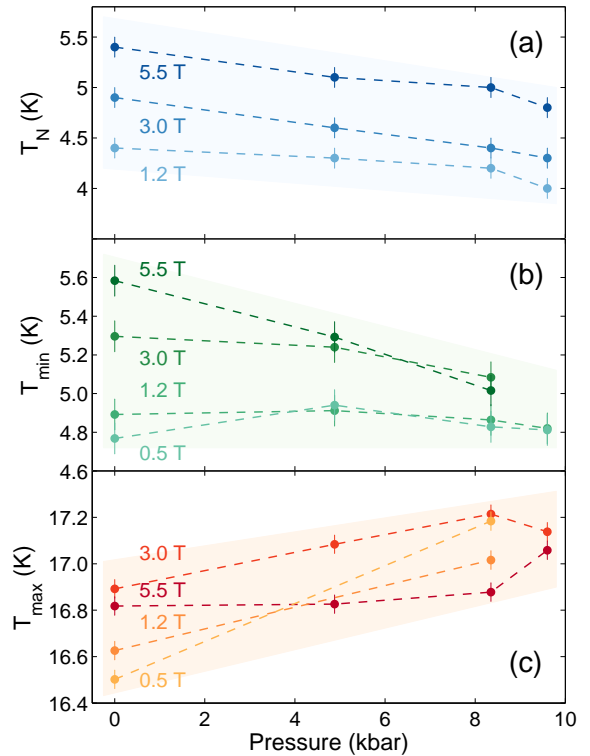


FIG. 6. (Color online) T_N (a), T_{\min} (b), and T_{\max} (c) vs. applied pressure for a selection of magnetic field values. While the first two show a decreasing trend with pressure, T_{\max} exhibits an opposite behavior (shaded areas). A compensation of pressure and magnetic-field effects (especially at higher fields) prevented a more detailed analysis.

denote the changes of the volume thermal-expansion coefficient and of the specific heat at constant pressure across the transition to 3D AFM order.

In Eq. 3 the product TV_m is always positive, while from specific-heat measurements it is known that $\Delta C_p > 0$ for $\text{Cu}(\text{pz})_2(\text{ClO}_4)_2$.⁸ A negative value of dT_N/dp requires that $\Delta\beta$ is negative, but this has not been confirmed by any experiment yet. At any rate, as we pointed out above, the results of NMR experiments to be described below, confirm that T_N decreases monotonously with increasing pressure.

The occurrence of a negative $\Delta\beta$ and hence $dT_c/dp < 0$ across a phase-boundary is quite common for conventional superconductors and is usually interpreted as being due to an enhanced stiffness of the crystal lattice at higher pressure. In our case, T_N depends primarily on the strength of the intraplane (J) and interplane (J_{int}) exchange interactions between the Cu ions. For $J_{\text{int}} = 0$, i.e., the ideal 2D Heisenberg AFM situation, a transition to an ordered state is not expected for $T > 0$.²⁷ For $J_{\text{int}} \neq 0$, it was concluded from QMC simulations that the relation between T_N and J_{int}/J can be described quite accurately by:²⁸

$$T_N = \frac{4\pi\rho_S}{b - \ln(J_{\text{int}}/J)}. \quad (4)$$

Here $\rho_S = 0.138J$ is the spin-stiffness parameter and $b = 2.43$ for $S = 1/2$. Thus the observed reduction of T_N under pressure requires that either J or the ratio J_{int}/J decreases. The second requirement can be fulfilled if J increases with pressure, in contrast with the first requirement or, if J_{int} is reduced substantially, hardly to be expected upon increasing pressure. According to the data shown in Fig. 6(b),

$T_{\max}(p)$ and, therefore, $J(p)$ exhibit a trend of enhancement with increasing pressure. Taken together, these observations imply that on the basis of the presently available data, there is no straightforward explanation for the $dT_N/dp < 0$ behavior.

B. NMR measurements

In what follows we describe a ^{35}Cl NMR study aimed at exploring the low-temperature magnetic order in $\text{Cu}(\text{pz})_2(\text{ClO}_4)_2$. For this purpose a single-crystal specimen was mounted on the sample-holder and aligned with its hard axis a parallel to the externally applied static field $\mu_B H = 7.066\text{ T}$.

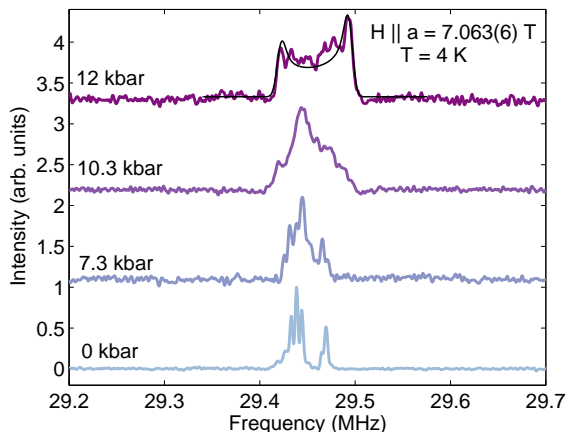


FIG. 7. (Color online) Low-temperature ^{35}Cl NMR lineshapes at four different pressures. The progressive line broadening with pressure suggests the development of an incommensurate magnetic structure at 12 kbar. The black line represents a model calculation (see text).

From previous investigations it is known that in a field of approximately 0.5 T, $\text{Cu}(\text{pz})_2(\text{ClO}_4)_2$ exhibits a spin-flop transition below T_N , resulting in a bicritical point in the (H, T) phase diagram.⁹ In such a low magnetic field, the S/N ratio of the NMR experiments, however, does not allow for accumulating reliable data in a reasonable amount of time and, therefore, this transition cannot be monitored via ^{35}Cl NMR.

The onset of the AFM order in zero field was first established at $T_N = 4.21\text{ K}$ via μSR experiments.⁷ Later on it was reported that the boundary fixing T_N extends up to higher fields of at least 12 T with $dT_N/dH > 0$.⁸ For our measurements we have chosen an external field of approximately 7 T (see above). By inserting the specimen into a high-pressure cell, we were able to monitor the pressure effects on T_N , from ambient pressure up to $p = 12\text{ kbar}$.

In Fig. 7 we display a selection of ^{35}Cl NMR lines measured at 4 K, i.e., below T_N , at four different externally applied hydrostatic pressures of 0.0, 7.3, 10.3, and 12 kbar. The NMR lineshapes reflect the local distribution of magnetic fields and hence provide information on the magnetic structure of the ordered phase. Due to two magnetically inequivalent sites, at zero pressure the spectra feature two main peaks, similar to those observed above T_N (not shown), where the absence of quadrupole splitting reflects the high (tetrahedral) symmetry of the perchlorate (ClO_4^-) counterions. A lowering of the symmetry below

T_N , gives rise to a tiny (5.6 kHz) quadrupole splitting in at least one of the sites which, by taking into account the ^{35}Cl quadrupole moment, $Q = -8.2 \times 10^{-30}\text{ m}^2$, implies an electric field gradient $eq \sim 2 \times 10^{19}\text{ V/m}^2$. The separate peaks observed at zero applied pressure gradually broaden and mix upon increasing pressure. The broadening of the lines and the growing irregularity of their shapes indicate a growing complexity of the local magnetization. It is conceivable that the soft ClO_4 ligands bridging the Cu-ion planes cause internal deformations of the unit cells, thereby enhancing the complexity of the two AFM sublattices and lead to a commensurate-to-incommensurate crossover. Indeed, the lineshape at 12 kbar is reminiscent of an incommensurate magnetic structure. A simplified model (see, e.g., Ref. 29 and 30) with a magnetic splitting $\Delta_M = 69\text{ kHz}$ (0.165 T) reproduces the experimental data reasonably well. In addition, the asymmetric line shape indicates a bunching of the Cu^{2+} magnetic moments along the applied field direction.

A study of the Cu(II)-based coordination network compound $\text{CuF}_2(\text{H}_2\text{O})_2(\text{pz})$ has already shown that hydrostatic pressure can drastically change the magnetic properties of this class of materials.³¹ In particular, since some bonds and bridges are *softer* and others more *rigid*, pressure can induce non-isotropic deformations, including both axial and angular distortions. Similarly, in the $\text{Cu}(\text{pz})_2(\text{ClO}_4)_2$ case, the interlayer interactions and the perchlorate gegenanions are expected to be more sensitive to distortions than the pyrazine bridges. This would imply an increase in T_N with pressure, reflecting a reduced interlayer distance, an increased number of nearest neighbors and, as a consequence, a reduction of quantum fluctuations. Experimental data, as those shown in Fig. 8, however, clearly contradict this hypothesis.

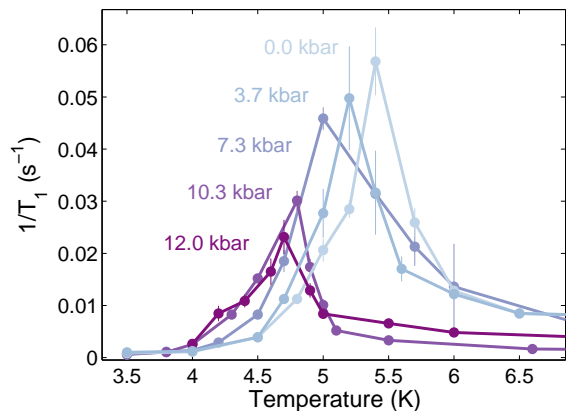


FIG. 8. (Color online) The $1/T_1$ vs. T dependence shows clear peaks at T_N . As the pressure increases the peaks become less prominent (slower spin-lattice relaxation times) and shift toward lower temperatures. Lines are guides to the eye.

The NMR spin-lattice relaxation rate $T_1(T)$ is expected to exhibit a peak at the transition to magnetic order.³² This is clearly confirmed in our case by the data displayed in Fig. 8, which show $1/T_1(T)$ for different applied pressures. The covered temperature range from 3.5 to 8 K was sufficient to adequately explore the accessible phase boundary. The spin-lattice relaxation times T_1 were obtained by means of the inversion-recovery method. The magnetization recovery was fitted using:³³

$$M_z(t)/M_0 = 1 - f [0.9 \cdot e^{-(6t/T_1)^\lambda} + 0.1 \cdot e^{-(t/T_1)^\lambda}], \quad (5)$$

an equation valid for spin- $3/2$ nuclei. Here M_0 is the saturation value of the nuclear magnetization, f is an amplitude parameter (ideally 2 for a complete inversion), while the stretching coefficient λ accounts for the distribution of the spin-lattice relaxation times around a characteristic value T_1 . Usually $\lambda = 1$ at high temperatures indicates a well-defined single spin-lattice relaxation rate $1/T_1$. At lower temperatures, λ often starts to decrease, indicating a growing distribution of $1/T_1$ values. In our case $\lambda(T)$ is of the order of 1 at the selected pressures across the covered temperature range. We notice that the intensity of the peaks, corresponding to the fastest relaxation times, is less prominent as the pressure increases. This observation indicates that with increasing pressure, the phase boundary is less well defined and/or the onset of incommensurate magnetism occurs, a feature also suggested by the line-shapes (see above). The $T_N(p)$ plot shown in Fig. 9 reveals a linearly decreasing T_N , characterized by a slope $dT_N/dp = -0.050(8)$ K/kbar.

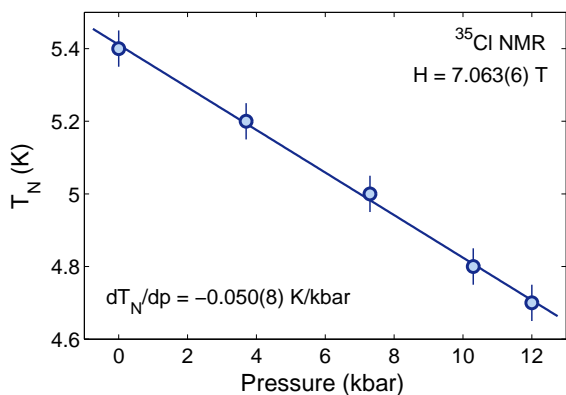


FIG. 9. (Color online) T_N dependence on applied pressure exhibits a decreasing trend with a $dT_N/dp = -0.050(8)$ K/kbar slope. The linear-fit approximation is acceptable within this range of pressures.

Two factors may account for the observed behavior: (i) the intrinsic rhombic distortion of the Cu sublattice, due to a small 0.3% difference between the 2D lattice diagonals, causes an in-plane anisotropy,⁹ and (ii) the anisotropic response of the system under hydrostatic pressure. Both of them result in angular deformations which quantitatively oppose the AFM ordering and shift the magnetic transition towards lower temperatures.

IV. ACCESSIBILITY OF THE BKT PHASE TRANSITION

As we argued above, the temperature dependence of magnetization $M(T)$ in $\text{Cu}(\text{pz})_2(\text{ClO}_4)_2$ indicates a crossover from an isotropic Heisenberg-AFM to an XY-model behavior at low temperatures. An XY phase is expected to be unstable with respect to a topological Berezinskii-Kosterlitz-Thouless (BKT) transition^{13,14} at $T_{\text{BKT}} < T_{\text{XY}}$. Below T_{BKT} , a quasi-long range order (QLRO) is established, where the spins are aligned and the correlation-function decays with a power law, while at $T > T_{\text{BKT}}$, a disordered high-temperature phase with exponentially decaying correlations is adopted. Although in the QLRO phase, quantum fluctuations are strong enough to destroy any long-range order, when the alignment of a spin changes, the nearby spins can still follow the new align-

ment, hence preserving the local order. The vortices, a topologically stable arrangement of spins, lower the correlation of the system: at temperatures below the topological transition they exist in vortex-antivortex bound states with zero net vorticity.³⁴ On the other hand, above the transition, a proliferation of unbound vortices occurs. As reported in the literature, QMC simulations regarding the two-dimensional XY model allow for an evaluation of the numerical value of T_{BKT} by²²

$$T_{\text{BKT}} = 4\pi\rho_s(1 - 0.491\Delta_{\text{XY}})/\ln(419/\Delta_{\text{XY}}), \quad (6)$$

with ρ_s defined as in Eq. (4). Since $T_{\text{BKT}} \propto 1/\ln(1/\Delta_{\text{XY}})$, a negligibly small decrease of T_{BKT} is expected when $\Delta_{\text{XY}} \rightarrow 0$, even at low Δ_{XY} values. For instance, $k_{\text{B}}T_{\text{BKT}}$ decreases only marginally (from $\sim 0.285J$ to $0.25J$) upon a fivefold reduction of Δ_{XY} (from 0.1 to 0.02). By inserting the value of $\Delta_{\text{XY}} = 4.6 \times 10^{-3}$ for $\text{Cu}(\text{pz})_2(\text{ClO}_4)_2$ ²³ in Eq. (6), a relatively high value of $T_{\text{BKT}} = 2.75$ K is obtained. This, however, is still distinctly lower than T_N , implying that in $\text{Cu}(\text{pz})_2(\text{ClO}_4)_2$, due to the prior onset of the three-dimensional LRO antiferromagnetic phase, the BKT phase transition cannot be accessed experimentally under the present circumstances. Extremely well separated Cu(II)-ion layers have recently been identified in the compound $[\text{Cu}(\text{pz})_2(2\text{-hydroxypyridine})_2](\text{ClO}_4)_2$.³⁵ The reported intralayer coupling $J/k_{\text{B}} \simeq 8$ K and a correspondingly low value of the interlayer coupling $J'/J \leq 0.05\%$ suggest reductions of both T_N and T_{BKT} to below 2 K. According to Ref. 35, the compound does not order magnetically above 1.8 K. The possibility that in this case $T_{\text{BKT}} > T_N$ cannot be ruled out and should be checked experimentally.

V. SUMMARY AND CONCLUSIONS

The two-dimensional spin- $1/2$ square-lattice antiferromagnet $\text{Cu}(\text{pz})_2(\text{ClO}_4)_2$ was studied by means of SQUID magnetometry and ^{35}Cl NMR at different magnetic fields and hydrostatic pressures, which allowed for a mapping of the $[H, T]$ and $[p, T]$ phase diagrams up to 7 T and 12 kbar, respectively. We argue that the observed increase of the 3D ordering (T_N) and the XY crossover (T_{XY}) temperatures in large applied magnetic fields is due to both an enhancement of the effective XY anisotropy and the quenching of quantum fluctuations. Taken together, the data shown in Fig. 4 and Fig. 6 imply some degree of compensation between the effects of external magnetic field and external hydrostatic pressure. We speculate that, while the field quenches the fluctuations by enhancing the XY anisotropy, the increasing pressure opposes this trend by canting the electronic in-plane orbitals, thereby, modifying the spin-density distribution. Causes for the steady decrease of T_N with increasing pressure are, most likely, a small intrinsic in-plane rhombic distortion of the Cu-ion squares and a growing pressure-induced anisotropy. Both effects result in anisotropic angular deformations which oppose the AFM ordering and shift the 3D transition towards lower temperatures.

Even though the interlayer couplings induce a 3D AFM transition at nonzero temperatures, they do not significantly influence the trend of T_N under pressure. The main influence in tuning the transition temperature seems to be exerted by the planar deformation. It consists in the enhancement of the already documented weak in-plane frus-

tration of $\text{Cu}(\text{pz})_2(\text{ClO}_4)_2$, whereby the geometrical distortion of the square lattice at higher pressures modifies the relative weight of the NN and NNN terms in the Hamiltonian (Eq. 2), thus enhancing the quantum fluctuations which oppose the AFM order.

ACKNOWLEDGMENTS

This work was financially supported in part by the Schweizerische Nationalfonds zur Förderung der Wissenschaftlichen Forschung (SNF) and the NCCR research pool MaNEP of SNF.

* Corresponding author: tshiroka@phys.ethz.ch

- 1 T. M. Rice, “Low dimensional magnets,” in *High Magnetic Fields*, edited by C. Berthier, L. P. Lévy, and G. Martinez (Springer Verlag, Berlin, 2001) Chap. 5, pp. 139–160.
- 2 S. Sachdev, “Quantum magnetism and criticality,” *Nature Phys.* **4**, 173–185 (2008).
- 3 K. Di, S. X. Feng, S. N. Piramanayagam, V. L. Zhang, H. S. Lim, S. C. Ng, and M. H. Kuok, “Enhancement of spin-wave nonreciprocity in magnonic crystals via synthetic antiferromagnetic coupling,” *Sci. Rep.* **5**, 10153 (2015).
- 4 Y.-A. Soh and R. K. Kummamuru, “Spintronics in antiferromagnets,” *Phil. Trans. R. Soc. A* **369**, 3646–3657 (2011).
- 5 C. P. Landee and M. M. Turnbull, “Recent developments in low-dimensional copper(II) molecular magnets,” *Eur. J. Inorg. Chem.* **2013**, 2266–2285 (2013).
- 6 L. D. Landau and E. M. Lifshitz, *Statistical Physics I* (Pergamon Press, Oxford, 1980) Chap. 14, pp. 456–460.
- 7 T. Lancaster, S. J. Blundell, M. L. Brooks, P. J. Baker, F. L. Pratt, J. L. Manson, M. M. Conner, F. Xiao, C. P. Landee, F. A. Chaves, S. Soriano, M. A. Novak, T. P. Papageorgiou, A. D. Bianchi, T. Herrmannsdörfer, J. Wosnitzer, and J. A. Schlueter, “Magnetic order in the $S = 1/2$ two-dimensional molecular antiferromagnet copper pyrazine perchlorate $\text{Cu}(\text{Pz})_2(\text{ClO}_4)_2$,” *Phys. Rev. B* **75**, 094421 (2007).
- 8 N. Tsyrlin, F. Xiao, A. Schneidewind, P. Link, H. M. Rønnow, J. Gavilano, C. P. Landee, M. M. Turnbull, and M. Kenzelmann, “Two-dimensional square-lattice $S = 1/2$ antiferromagnet $\text{Cu}(\text{pz})_2(\text{ClO}_4)_2$,” *Phys. Rev. B* **81**, 134409 (2010).
- 9 K. Yu. Povarov, A. I. Smirnov, and C. P. Landee, “Switching of anisotropy and phase diagram of the Heisenberg square-lattice $S = 1/2$ antiferromagnet $\text{Cu}(\text{pz})_2(\text{ClO}_4)_2$,” *Phys. Rev. B* **87**, 214402 (2013).
- 10 J. Darriet, M. S. Haddad, E. N. Duesler, and D. N. Hendrickson, “Crystal structure and magnetic properties of bis(pyrazine)copper(II) perchlorate, $\text{Cu}(\text{pyz})_2(\text{ClO}_4)_2$, a two-dimensional Heisenberg antiferromagnet,” *Inorg. Chem.* **18**, 2679–2682 (1979).
- 11 S. Vela, J. Jornet-Somoza, M. M. Turnbull, R. Feyerherm, J. J. Novoa, and M. Deumal, “Dividing the spoils: Role of pyrazine ligands and perchlorate counterions in the magnetic properties of bis(pyrazine)diperchlorate copper(II), $[\text{Cu}(\text{pz})_2](\text{ClO}_4)_2$,” *Inorg. Chem.* **52**, 12923–12932 (2013).
- 12 The considerable T_N values even for modest or negligible inter-to-intralayer coupling ratios, have a semi-empirical explanation from Monte Carlo simulations, which indicate an almost constant T_N behavior even at small J' values [see Eq. (4)].²⁸ A suitable framework is provided by the self-consistent spin-wave theory of layered magnets with a weak interlayer coupling and magnetic anisotropy.^{8,36}
- 13 V. L. Berezinskii, “Destruction of long-range order in one-dimensional and two-dimensional systems possessing a continuous symmetry group. II. Quantum systems,” *Zh. Eksp. Teor. Fiz.* **61**, 1144–1156 (1971), [*Sov. Phys. JETP* **34**, 610–616 (1972)].
- 14 J. M. Kosterlitz and D. J. Thouless, “Ordering, metastability and phase transitions in two-dimensional systems,” *J. Phys. C: Solid State Phys.* **6**, 1181 (1973).
- 15 F. M. Woodward, P. J. Gibson, G. B. Jameson, C. P. Landee, M. M. Turnbull, and R. D. Willett, “Two-dimensional Heisenberg antiferromagnets: Syntheses, X-ray structures, and magnetic behavior of $[\text{Cu}(\text{pz})_2](\text{ClO}_4)_2$, $[\text{Cu}(\text{pz})_2](\text{BF}_4)_2$, and $[\text{Cu}(\text{pz})_2(\text{NO}_3)](\text{PF}_6)$,” *Inorg. Chem.* **46**, 4256–4266 (2007).
- 16 M. I. Eremets, *High pressure experimental methods* (Oxford University Press, Oxford, 1996).
- 17 A. P. Reyes, E. T. Ahrens, R. H. Heffner, P. C. Hammel, and J. D. Thompson, “Cuprous oxide manometer for high pressure magnetic resonance experiments,” *Rev. Sci. Instr.* **63**, 3120–3122 (1992).
- 18 M. J. Clark and T. F. Smith, “Pressure dependence of T_c for lead,” *J. Low Temp. Phys.* **32**, 495–503 (1978).
- 19 M. E. Lines, “The quadratic-layer antiferromagnet,” *J. Phys. Chem. Solids* **31**, 101–116 (1970).
- 20 J.-K. Kim and M. Troyer, “Low temperature behavior and crossovers of the square lattice quantum Heisenberg antiferromagnet,” *Phys. Rev. Lett.* **80**, 2705 (1998).
- 21 B. Bauer *et al* (ALPS collaboration), “The ALPS project release 2.0: Open source software for strongly correlated systems,” *J. Stat. Mech.* **2011**, P05001 (2011).
- 22 H.-Q. Ding, “Could in-plane exchange anisotropy induce the observed antiferromagnetic transitions in the undoped high- T_c materials?” *Phys. Rev. Lett.* **68**, 1927–1930 (1992).
- 23 F. Xiao, F. M. Woodward, C. P. Landee, M. M. Turnbull, C. Mielke, N. Harrison, T. Lancaster, S. J. Blundell, P. J. Baker, P. Babkevich, and F. L. Pratt, “Two-dimensional XY behavior observed in quasi-two-dimensional quantum Heisenberg antiferromagnets,” *Phys. Rev. B* **79**, 134412 (2009).
- 24 A. Cuccoli, T. Roscilde, R. Vaia, and P. Verrucchi, “Detection of XY behavior in weakly anisotropic quantum antiferromagnets on the square lattice,” *Phys. Rev. Lett.* **90**, 167205 (2003).
- 25 R. Gupta, J. DeLapp, G. G. Batrouni, G. C. Fox, C. F. Baillie, and J. Apostolakis, “Phase transition in the 2D XY model,” *Phys. Rev. Lett.* **61**, 1996–1999 (1988).
- 26 A. B. Pippard, *Elements of Classical Thermodynamics* (Cambridge University Press, Cambridge, 1966) Chap. 9.
- 27 N. D. Mermin and H. Wagner, “Absence of ferromagnetism or antiferromagnetism in one- or two-dimensional isotropic Heisenberg models,” *Phys. Rev. Lett.* **17**, 1133–1136 (1966).
- 28 C. Yasuda, S. Todo, K. Hukushima, F. Alet, M. Keller, M. Troyer, and H. Takayama, “Néel temperature of quasi-low-dimensional Heisenberg antiferromagnets,” *Phys. Rev. Lett.* **94**, 217201 (2005).
- 29 R. Blinc, “Magnetic resonance and relaxation in structurally incommensurate systems,” *Phys. Rep.* **79**, 331–398 (1981).
- 30 A. A. Gippius, A. S. Moskvina, and S.-L. Drechsler, “Spin polarization of the magnetic spiral in NaCu_2O_2 as seen by nuclear magnetic resonance spectroscopy,” *Phys. Rev. B* **77**, 180403 (2008).
- 31 G. J. Halder, K. W. Chapman, J. A. Schlueter, and J. L. Manson, “Pressure-induced sequential orbital reorientation in a magnetic framework material,” *Angew. Chem. Int. Ed.* **50**, 419–421 (2011).
- 32 F. Borsa, “Phase transitions and critical phenomena in solids,” in *eMagRes*, edited by R. K. Harris and R. E. Wasylshen (John Wiley & Sons, Hoboken, NJ, 2007).
- 33 A. F. McDowell, “Magnetization-recovery curves for quadrupolar spins,” *J. Magn. Reson., Ser. A* **113**, 242–246 (1995).
- 34 A. W. Sandvik, “Computational studies of quantum spin systems,” *AIP Conf. Proc.* **1297**, 135 (2010).

- ³⁵ V. Selmani, C. P. Landee, M. M. Turnbull, J. L. Wikaira, and F. Xiao, “An extremely well isolated 2D-antiferromagnetic layer,” *Inorg. Chem. Commun.* **13**, 1399–1401 (2010).
- ³⁶ V. Yu. Irkhin, A. A. Katanin, and M. I. Katsnelson, “Self-

consistent spin-wave theory of layered Heisenberg magnets,” *Phys. Rev. B* **60**, 1082–1099 (1999).